ACS APPLIED MATERIALS & INTERFACES

Research Article

www.acsami.org

High-Efficiency $AgInS_2$-Modified ZnO Nanotube Array Photoelectrodes for All-Solid-State Hybrid Solar Cells

Jianhua Han,[†] Zhifeng Liu,*[,†] Keying Guo,[†] Jing Ya,[†] Yufeng Zhao,*[,‡] Xueqi Zhang,[†] Tiantian Hong,[†] and Junqi Liu[†]

[†]School of Materials Science and Engineering, Tianjin Chengjian University, Tianjin 300384, China

[‡]Department of Environmental and Chemical Engineering, Yanshan University, Qinhuangdao 066004, China

ABSTRACT: Highly ordered $AgInS_2$-modified ZnO nanoarrays were fabricated via a low-cost hydrothermal chemical method, and their application as all-solid-state solar cells was also tested. A sensitizer and a buffer layer were developed around the surface of ZnO nanotubes in the preparation process, and this method is easily be manipulated to produce uniform structure. In this structure, the ZnO served as direct electron transport path, the ZnS as the buffer layer, and the ternary sensitizer $AgInS_2$ as absorber and outer shell. The novel all-solid-state hybrid solar cells (ITO/ZnO/ZnS/$AgInS_2$/P3HT/Pt) showed improved short-circuit current density (J_{sc}) of 7.5 mA/cm^2, open-circuit voltage (V_{oc}) of 512 mV, giving rise to a power conversion efficiency of 2.11%, which is the relatively highest value ever reported for ZnO-based all-solid-state hybrid solar cells. This better result is attributed to the improved absorption spectrum, high speed of photoinduced charge transmission velocity, and appropriate gradient energy gap structure, which implies a promising application in all-solid-state solar cells.

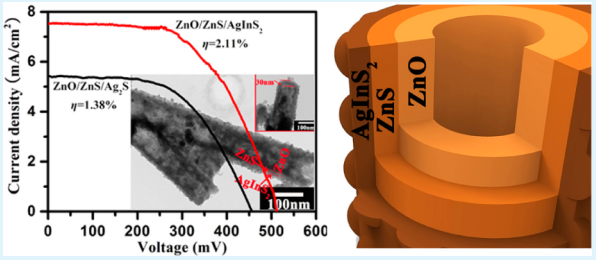

KEYWORDS: *highly ordered, $AgInS_2$, buffer layer, all-solid-state, solar cell*

1. INTRODUCTION

As a kind of potential photoelectrode material for solar cells, metal oxides have received extensive attention in recent years due to their low-cost, versatile applicability and environmental stability.[1−3] Nevertheless, the absorption of traditional metal oxides (such as ZnO[4,5] and TiO_2[6,7]) is limited to UV region because of the large band gap, which restricts their practical applications. Therefore, considerable efforts have been made to extend the absorption spectrum to the visible light region by sensitizing with quantum dots (QDs).[8,9] It is well-known that the most efficient technique QDs sensitization for metal oxides is to create core/shell nanostructure, which can offer controlled performance and protect the core materials.[10] Though CdS, PbS, etc., QDs can provide high activity in solar cells, their high toxicity becomes a main concern, which presents a serious threat to human health and the environment.[11] All-solid-state inorganic−organic hybrid solar cell based on sensitizer modified metal oxides photoanode shows tremendous potential because of its (i) low-cost fabricating; (ii) versatile applicability; (iii) environmental stability. In 2012, Li et.al reported TiO_2-coated ZnO nanorods/P3HT solar cell with a power conversion efficiency of 0.76%,[12] in 2013, Chen et.al reported dye-modified ZnO nanorod array/P3HT hybrid solar cell with a power conversion efficiency of 1.16%.[13]

Recently, environmentally friendly ternary semiconductor nanocrystals such as $AgInS_2$ have emerged as a possible alternative to the toxic light absorbing materials currently in use. As an attractive visible-light absorber materials for solar energy conversion systems, the ternary semiconductor $AgInS_2$ with a band gap of 1.8 eV is chosen as outer shell sensitizer due to its low toxicity and large absorption coefficient in the visible light region.[14,15] To the best knowledge, although $AgInS_2$ has demonstrated high photoelectrical activity, there are few reports about the photoelectrodes of $AgInS_2$ served as sensitizer in solar cells. In 2013, Liu et.al reported a facile synthesis of $AgInS_2$ hierarchical flowerlike nanoarchitectures composed of ultrathin nanowires,[16] Mamidala et al. prepared anisotropic CdS-$AgInS_2$ nanocrystals, and investigated their photoconductive properties.[17]

In this study, double-walled ZnO/ZnS/$AgInS_2$ NT arrays were first prepared via a low-cost facile hydrothermal chemical conversion method based on ion-exchange, and then applied in inorganic−organic hybrid solar cells. As we all know, most conventional methods for the fabrication of core/shell structure, like chemical bath deposition (CBD) and electrodeposition, could introduce many clusters and defects into the nanostructures, and thus degrade the photoelectric performance of the obtained samples.[18] Being different with the traditional methods, the hydrothermal chemical conversion method is easy to be manipulated and form uniform structure without destroying the original backbone, which can decrease defects and enhance the light-harvesting ability of the photoelectrodes. Meanwhile, it can provide a relatively stable environment for related reaction process to support the

Received: July 21, 2014
Accepted: September 11, 2014
Published: September 11, 2014

   dx.doi.org/10.1021/am5047813 | ACS Appl. Mater. Interfaces 2014, 6, 17119−17125

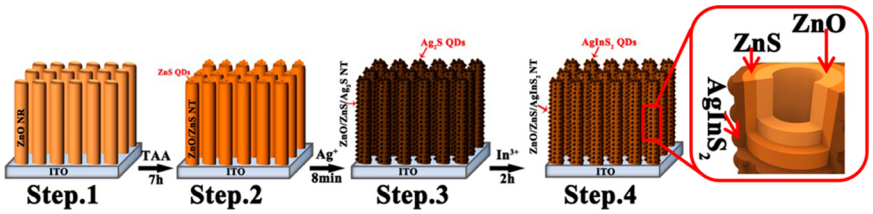

Figure 1. Schematic illustration for the synthesis ZnO/ZnS/$AgInS_2$ NT arrays step by step.

fabrication of the desirable products. Hence, hydrothermal chemical conversion method based on ion-exchange is served as the ideal way to regulate the chemical compositions and structure of samples. Practically, a buffer layer of ZnS can be retained when a sensitizer layer of $AgInS_2$ formed on the surface of ZnO nanoarrays during the chemical conversion process. Strikingly, the all-solid-state hybrid solar cell (ITO/ZnO/ZnS/$AgInS_2$/P3HT/Pt) based on ZnO/ZnS/$AgInS_2$ shows an impressive photovoltaic performance with a J_{sc} of 7.5 mA/cm^2, V_{oc} of 512 mV and a power conversion efficiency of 2.11%, because of the improved absorption spectrum in the visible-light region and appropriate gradient energy gap structure.

2. EXPERIMENTAL SECTION

2.1. Preparation of ZnO NR Arrays. The ZnO NR arrays were fabricated on the indium tin oxide (ITO) glass substrates using hydrothermal method, which consists of substrate pretreatment and hydrothermal growth.[18,19] The ITO glass substrates were ultrasonically rinsed for 0.5 h in acetone, isopropyl alcohol, and ethanol solution, respectively. The ZnO seed layers were first deposited on ITO substrates by a sol–gel and dip-coating method. After heat treatment at 400 °C for 1 h, the ITO coated with seed layers was immersed in the aqueous solution containing 0.05 M zinc nitrate ($Zn(NO_3)_2$) and 0.05 M hexamethylenetetramine (HMTA) at 90 °C for 4 h. Fabricated ZnO NR arrays were washed with deionized water and dried in air.

2.2. Preparation of ZnO/ZnS/$AgInS_2$ NT Arrays. To obtain ZnO/ZnS/$AgInS_2$ NT arrays, we first prepared the ZnO/ZnS/Ag_2S NT arrays via chemical etching and anion exchange process by using ZnO NR arrays as reactive templates. To elaborate, the ZnO NRs were immersed in aqueous solutions containing 0.1 M thiacetamide (TAA) at 90 °C for 7 h to prepare ZnO/ZnS core/shell arrays. The as-obtained samples were then washed with deionized water and dried in air. After that, 4 mg of silver nitrate ($AgNO_3$) was dissolved in 25 mL of deionized water. Arrays of ZnO/ZnS were immersed in the aforementioned solution and kept for 10 min at 28 °C to fabricate ZnO/ZnS/Ag_2S arrays. Finally, the samples were washed with deionized water and dried in air.

The obtained arrays of ZnO/ZnS/Ag_2S were further immersed in triethylene glycol (TEG) containing 0.006 g of indium chloride ($InCl_3$) in a Teflon-lined stainless steel autoclave. The autoclave was then sealed and maintained at 200 °C for 3 h to obtain ZnO/ZnS/$AgInS_2$ arrays, and naturally cooled to room temperature. The samples were washed with absolute ethanol for several times and finally dried in air.

2.3. Assembly of Inorganic–Organic Hybrid Solar Cells. Both the ZnO/ZnS/Ag_2S and ZnO/ZnS/$AgInS_2$ array films were spin-coated at 2500 rpm for 60 s with a regioregular-P3HT (poly-3-hexylthiophene) chlorobenzene solution. The above cycle was repeated several times in order to achieve the compact fill of P3HT. Then the state inorganic–organic hybrid solar cells were assembled by covered with platinum (Pt) sheet as counter electrodes.

2.4. Characterization. Morphology and structure of the samples were observed under HITACHI S-4800I field emission scanning electron microscope (FE-SEM) and HITACHI H-7650 transmission electron microscopy (TEM, 100 kV). The energy-dispersive spectrometer (EDS) spectra of the samples were also performed during the FE-SEM observation. X-ray diffraction (XRD) patterns of the samples were performed using a Rigaku D/max-2500 using Cu Kα radiation (λ = 0.154059 nm). Optical absorbance of the photoelectrodes was examined by DU-8B UV/vis double-beam spectrophotometer. Electrochemical impedance spectroscopy (EIS) of samples was performed with an electrochemical workstation (LK2005A, Tianjin, China). Photocurrent of the all-solid-state inorganic–organic hybrid solar cells was measured under irradiation of a xenon lamp with global AM 1.5 G condition, and photocurrent–voltage curves of the cells were obtained using a potentiostat. It should be noted that in order to lessen the errors on the efficiency measurements, five cell samples suited to each photoelectrode type were used.

3. RESULTS AND DISCUSSION

The ZnO/ZnS/$AgInS_2$ NT arrays were prepared mainly by hydrothermal chemical conversion method, and the reaction process is schematically illustrated in Figure 1. First, the hexagonal ZnO NR arrays were fabricated by a simple hydrothermal method (Step.1). In this step, the wurtzite ZnO seed layers were formed after sintering, on which ZnO seed layers would develop into ZnO NR arrays in the growth solution. It is generally known that chemical conversion method based on ion-exchange would occur spontaneously when there are large differences in the solubility product constants between the reactants and the products.[18,20] Hence, when the sample of ZnO arrays is immersed into a solution containing 0.05 M TAA, the sulfidation reaction of ZnO NR will take place because of the large difference between the solubility product constants (K_{sp}) of ZnO (6.8×10^{-17}) and ZnS (2.93×10^{-25}). At the beginning of sulfidation of ZnO NR in TAA solution, the large difference in K_{sp} of ZnO and ZnS indicate that S^{2-} produced from TAA hydrolyzes under 90 °C can bond with Zn^{2+} (eqs 1 and 2). In other words, the surface of ZnO NR will be sluggish dissolved when S^{2-} replace O^{2-} around the surface of ZnO NR for formed ZnS around the ZnO NR and the apex of ZnO NR (eq 3). The further reaction of ZnO with S^{2-} on the whole surface of the NR leads to the formation of a uniform shell of ZnS surrounding the ZnO when the reaction time reaches 7 h (step 2). Second, Ag_2S shell is obtained in step 3 via replacing part of Zn^{2+} by Ag^+ because of the large differences in K_{sp} between ZnS (2.93×10^{-25}) and Ag_2S (1.6×10^{-49}) (eq 4), and thus ZnS shell is partially converted to Ag_2S shell by the metal cation exchange process. In this step, the ZnO/ZnS/Ag_2S NT arrays were obtained by using ZnO/ZnS NT arrays as reactive templates, a buffer layer of ZnS and a binary sensitizer layer of Ag_2S was formed at the same time (Step 3). Finally, the $AgInS_2$ shell was obtained when Ag_2S react with enough In^{3+} in the triethylene glycol (TEG) solvent with high temperature (Step 4). Compared with other conventional synthesis routes, this chemical conversion method based on ion-exchange is simple, low-cost, and eco-friendly. Best of all, it can fabricate a uniform core/shell structure array. The structure of as-obtained ZnO/ZnS/$AgInS_2$ NT is illustrated in Figure 1.

It should be noticed that the pH value of the whole hydrothermal process is about 5, as an amphoteric oxide, ZnO NR can react with H^+ in acid solution and the products are soluble salts (eq 5). Thus, the chemical etching process will take place when the sample of ZnO NR arrays is immersed in the acid solution.[21] While, the etching process is selective and mainly focused on the inner of NR, it was owing to the polar plane (002) of wurzite ZnO crystal with high surface energy is instable, and the nonpolar planes parallel to *c*-axis are the most stable planes with a lower surface energy. Hence, the etching rate of the polar plane (the top plane of ZnO) is faster than that of nonpolar planes (the lateral plane of ZnO).[22,23] With the increasing etching time, the depth of the NT gradually increased. Finally, the ZnO/ZnS/$AgInS_2$ NT arrays were fabricated successfully.

$$CH_3CSNH_2 + H_2O \rightarrow CH_3CONH_2 + H_2S \quad (1)$$

$$H_2S \rightarrow 2H^+ + S^{2-} \quad (2)$$

$$ZnO + S^{2-} + H_2O \rightarrow ZnS + 2OH^- \quad (3)$$

$$ZnS + 2Ag^+ \rightarrow Ag_2S + Zn^{2+} \quad (4)$$

$$ZnO + 2H^+ \rightarrow Zn^{2+} + H_2O \quad (5)$$

The morphology of as-obtained products was characterized by FE-SEM. Typical top-view SEM image of the as-obtained ZnO/ZnS/$AgInS_2$ NT arrays is shown in Figure 2a, it can be seen

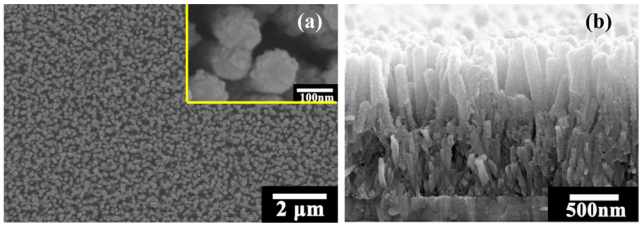

Figure 2. (a) Top-view SEM image and (inset) enlarged-view SEM image; (b) side-view SEM image of ZnO/ZnS/$AgInS_2$ NT arrays.

that the diameter of NTs is about 120 nm. It is obvious that well-aligned vertically ZnO/ZnS/$AgInS_2$ arrays were uniformly and densely covered on the ITO substrate (Figure 2 (a)), from the enlarged view in the inset of Figure 2a, it can be seen that some nanoparticles accumulated on the top of the NTs. Figure 2b shows the side-view SEM image of the ZnO/ZnS/$AgInS_2$ arrays, the length of the NTs is measured to be approximately 1.4 μm. It can be seen that the surface and the length of NT are relatively smooth and uniform, which agrees with the hypothesis that the reaction is based on ion-exchanging without destroying the original nanostructure and the backbone.

Figure 3a presents the middle part-TEM image and the inset of Figure 3a shows the top part-TEM image of the ZnO/ZnS/$AgInS_2$ NT arrays. It is clearly demonstrated that the as-prepared samples are composed of the uniform hollow structure with inner diameters of ~60 nm and the wall is as thick as about ~30 nm. It can be seen that the wall of sample consists of three layers, and the surface looks like accumulation of plenty of nanoparticles. The surface of NT appears relatively smooth and uniform, indicating that the chemical conversion based on ion-exchange without destroying the original structure. High-resolution TEM image of ZnO/ZnS/$AgInS_2$ NT is shown in Figure 3b, the fringe spacing of 0.13, 0.25, and

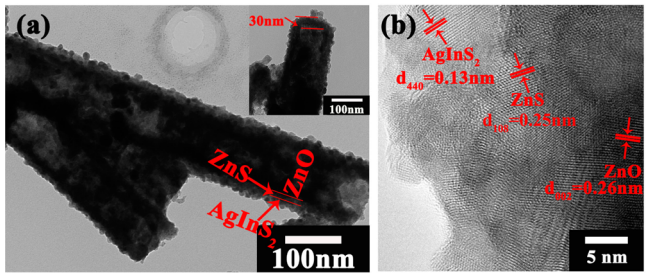

Figure 3. (a) Middle part TEM (inset: top part) and (b) HRTEM images of ZnO/ZnS/$AgInS_2$ NT arrays.

0.26 nm in Figure 3b matches well to the interplanar spacing of the (440), (108), and (002) lattice plane of $AgInS_2$, ZnS, and ZnO, respectively. These results provide credible evidence for the chemical composition of the ZnO/ZnS/$AgInS_2$ NT arrays, and further confirm that ZnO/ZnS/$AgInS_2$ NT arrays are prepared successfully, in which ZnO is the core, ZnS is the interlayer and the $AgInS_2$ is the shell with the distribution of $AgInS_2$ nanoparticles randomly over the surface. To further investigate the forming mechanism of ZnO/ZnS/$AgInS_2$ NTs, TEM images of ZnO NRs, ZnO/ZnS NTs, ZnO/ZnS/Ag_2S NTs, and ZnO/ZnS/$AgInS_2$ NTs were texted (Figure 4a–d).

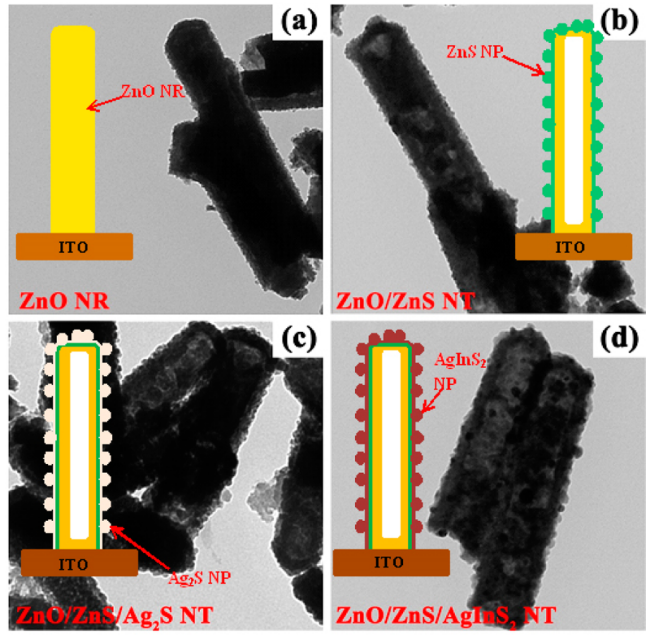

Figure 4. TEM images and schematic illustration of (a) ZnO NR, (b) ZnO/ZnS NT, (c) ZnO/ZnS/Ag_2S NT, and (d) ZnO/ZnS/$AgInS_2$ NT.

As shown in Figure 4, the chemical etching process was occurred when the ZnO NRs immersed in the TAA solution, finally, ZnO/ZnS NTs films with thin-wall were prepared. Then, the ZnS shell was partially converted to Ag_2S shell based on the metal cation exchange process, because of the large differences in K_{sp} between ZnS and Ag_2S, and ZnO/ZnS/Ag_2S NTs was obtained. Finally, the $AgInS_2$ shell was obtained when Ag_2S react with enough In^{3+} in the TEG with high temperature, and the products of ZnO/ZnS/$AgInS_2$ were achieved.

Figure 5 gives the XRD patterns of (a) the ZnO, (b) ZnO/ZnS, (c) ZnO/ZnS/Ag_2S, (d) ZnO/ZnS/$AgInS_2$, respectively. The corresponding XRD pattern of ZnO NRs is shown in

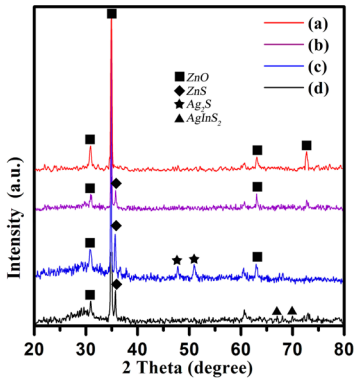

Figure 5. XRD patterns of (a) ZnO, (b) ZnO/ZnS, (c) ZnO/ZnS/Ag_2S, (d) ZnO/ZnS/$AgInS_2$.

Figure 5a, in comparison with the standard ZnO diffraction pattern (JCPDS, No. 36−1451), the as-obtained ZnO NRs are mainly grown along the (002) direction. Figure 5b presents the XRD pattern of the ZnO/ZnS NTs, in addition to ZnO, characteristic peaks of ZnS (JCPDS, No. 12−0688) appear, indicating that the as-obtained ZnO arrays have been converted to ZnO/ZnS core/shell nanoarrays already. The XRD pattern of ZnO/ZnS/Ag_2S NTs is given in Figure 5c, besides the diffraction peaks of ZnO and ZnS, more diffraction peaks are observed, which are indexed to Ag_2S (JCPDS, No. 65−2356). Figure 5d shows the XRD pattern of ZnO/ZnS/$AgInS_2$ NTs, some diffraction peaks of $AgInS_2$ (JCPDS, No.65−7332), ZnS, and ZnO are observed in this spectrum, indicating the formation of ZnO/ZnS/$AgInS_2$ composite structure. All the peaks of ZnO, ZnS, and $AgInS_2$ are reflected in this pattern, which implied that the Ag_2S shell was converted to $AgInS_2$ (Figure 5d). These results provide credible evidence for the chemical composition of the ZnO/ZnS/$AgInS_2$ NT arrays, and further confirm that the ZnS shell transforms partially to $AgInS_2$ shell, the double-walled ZnO/ZnS/$AgInS_2$ heterojunction arrays were prepared successfully. Figure 6 shows the EDS spectrum of (a) as-obtained ZnO/ZnS/Ag_2S and (b) ZnO/ZnS/$AgInS_2$. As shown in Figure 6, NTs consist of Ag, S, O, In, and Zn elements, whereas the other peaks (Si, Ca) are

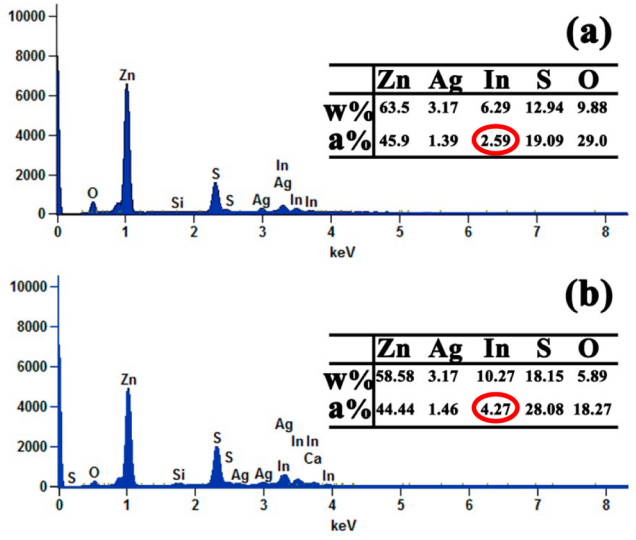

Figure 6. EDS patterns of the (a) ZnO/ZnS/Ag_2S, (b) ZnO/ZnS/$AgInS_2$.

originated from ITO glass. Compared the content of indium (In) in Figure 6b with that of Ag in Figure 6a, the increment of indium (In) is close to the content of Ag (Ag:In = 1:1), which is well-consistent with the XRD results.

The optical properties of ZnO, ZnO/ZnS, ZnO/ZnS/Ag_2S and ZnO/ZnS/Ag_2S/$AgInS_2$ were characterized by the UV−vis absorption spectra, which are shown in Figure 7. The inset (1−

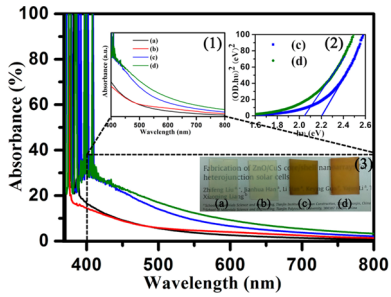

Figure 7. UV−visible light absorption spectra of samples. Inset (1): visible light absorption spectra of samples of (a) ZnO, (b) ZnO/ZnS, (c) ZnO/ZnS/Ag_2S, (d) ZnO/ZnS/$AgInS_2$. Inset (2): Curves of $(OD h\nu)^2$ versus $h\nu$ of (c) ZnO/ZnS/Ag_2S, (d) ZnO/ZnS/$AgInS_2$. Inset (3): Photographs of the samples of (a) ZnO, (b) ZnO/ZnS, (c) ZnO/ZnS/Ag_2S, (d) ZnO/ZnS/$AgInS_2$.

3) in Figure 7 display visible light absorption spectra of samples of (a) ZnO, (b) ZnO/ZnS, (c) ZnO/ZnS/Ag_2S, (d) ZnO/ZnS/$AgInS_2$; the band gap and the photographs of (a) ZnO, (b) ZnO/ZnS, (c) ZnO/ZnS/Ag_2S, and (d) ZnO/ZnS/$AgInS_2$, respectively. Compared with absorption of ZnO NRs, all the samples of ZnO/ZnS, ZnO/ZnS/Ag_2S, and ZnO/ZnS/$AgInS_2$ show a significant enhancement in visible light region, and the ZnO/ZnS/$AgInS_2$ shows the highest efficiency of visible light absorption (inset (1) of Figure 7). With the increasing of reaction time, the color of samples changes gradually step and step (inset (3) of Figure 7). The approximate band gap of ZnO/ZnS/Ag_2S and ZnO/ZnS/$AgInS_2$ are determined to be ∼2.20 and ∼2.05 eV, which is more suitable for the absorption of visible light than that of the single ZnO NR arrays (inset (2) of Figure 7). It can be concluded that $AgInS_2$ sensitizer enlarge notably the photo response spectrum to visible light, because of the appropriate energy band gap structure and the high optical absorption coefficient of $AgInS_2$.

The inorganic−organic hybrid solar cells based on ZnO NR, ZnO/ZnS/Ag_2S NT and ZnO/ZnS/$AgInS_2$ NT arrays were assembled using P3HT as hole conductor. The structure of all-solid-state inorganic−organic hybrid solar cells is shown in Figure 8. For ZnO/ZnS/$AgInS_2$/P3HT/Pt hybrid solar cells, ZnO provides electron transport pathway, ZnS serves as a buffer layer to optimize the band configuration of the structure, $AgInS_2$ is used for sensitizer, P3HT plays a role of hole conductor and light absorber,[3] Pt as the counter electrode. Figure 9 shows the current density−voltage (J−V) curves for the samples tested under the irradiation of a simulated sunlight (AM 1.5 G, 100 mW/cm^2). The parameters of the inorganic−organic hybrid solar cells based on ZnO NR arrays, ZnO/ZnS/Ag_2S NT arrays and ZnO/ZnS/$AgInS_2$ NT arrays are presented in Table 1. During the photocurrent measurements, the power conversion efficiency of cell is calculated by the following equations

$$\eta = (V_{oc} J_{sc} FF)/P_{in} \quad (6)$$

dx.doi.org/10.1021/am5047813 | ACS Appl. Mater. Interfaces 2014, 6, 17119−17125

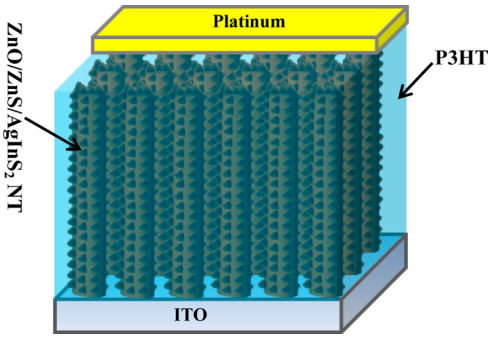

Figure 8. Schematic Diagram of inorganic–organic hybrid solar cell (ITO/ZnO/ZnS/$AgInS_2$/P3HT/Pt).

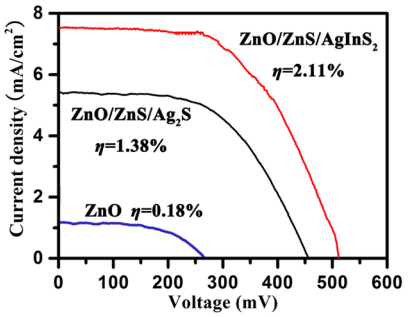

Figure 9. J–V curves of the ZnO, ZnO/ZnS/Ag_2S and ZnO/ZnS/$AgInS_2$ inorganic–organic hybrid solar cells under simulated AM 1.5 sunlight.

Table 1. Parameter of Inorganic–Organic Hybrid Solar Cells with Different Sensitizers

photoelectrode	V_{oc} (mV)	J_{sc} (mA cm^{-2})	FF (%)	η (%)
ZnO	269	1.2	55	0.18
ZnO/ZwnS/Ag_2S	456	5.4	56	1.38
ZnO/ZnS/$AgInS_2$	512	7.5	55	2.11

$$FF = V_{opt}J_{opt}/V_{oc}J_{sc} \quad (7)$$

where P_{in} is the power of incident white light, FF is fill factor, V_{opt} and J_{opt} are voltage and current for maximum power output, and V_{oc} and J_{sc} are open-circuit photovoltage and short-circuit photocurrent, respectively. The solar cell based on ZnO, ZnS/ZnS/Ag_2S and ZnO/ZnS/$AgInS_2$ arrays exhibits a short-circuit current density (J_{sc}) of 1.2 mA cm^{-2}, 5.4 mA cm^{-2} and 7.5 mA cm^{-2}, an open-circuit voltage (V_{oc}) of 269, 456, and 512 mV, and a fill factor (FF) of 0.55, 0.56, and 0.55, obtaining a power conversion efficiency (η) of 0.18, 1.38 and 2.11%, respectively (Table 1). Compared with the cell based on ZnO arrays, the cell using ternary Ag_2S as sensitizer displays increases in V_{oc}, J_{sc}, and η for 69.5, 350, and 667%, respectively; Compared with the cell based on ZnO/ZnS/Ag_2S arrays, the cell using ternary $AgInS_2$ as sensitizer displays increases in V_{oc}, J_{sc}, and η for 12.3, 38.9, and 52.3%, respectively.

It is believed that the optimized performance of the solar cells is attributed to several major factors, i.e., the efficiency of light-harvesting, charge injection and collection.[24,25] For the ZnO/ZnS/$AgInS_2$ nanostructure, a high efficiency of light-harvesting can be obtained by fabricating well-aligned NT arrays with high specific area served as the photoelectrodes of solar cells. Meanwhile, charge injection and collection properties can be enhanced by constructing appropriate gradient energy gap structure. The photons transfer process is shown in Figure 10, $AgInS_2$ nanoparticles on the NT surface can improve

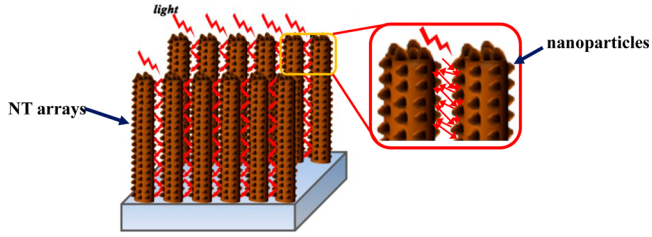

Figure 10. Schematic representation of the utilization of incident sunlight.

the light utilization efficiency. It can be seen that light would be reflected much more times among nanoparticles on the NT surface and among the NT arrays, such multiple reflections would extend the light propagation path, which is beneficial to the full utilization of incident light. Meanwhile, as a high light absorption coefficient materials in the visible regions, a layer of accumulated $AgInS_2$ nanoparticles can trap relatively more photons, and thus larger amount of photons would be utilized by the ZnO/ZnS/$AgInS_2$ NT arrays for producing electron/hole pairs. What is more, vertical ZnO arrays grown on the ITO glass can directly transport the photoinduced electrons with a high speed, which take full advantages of the excellent carrier transport performance of as-obtained samples.

Besides the effect of light utilization on the photoelectric performance, the rate of photoinduced electrons injection and transmission is a linchpin factor in the solar cells. In the ITO/ZnO/ZnS/$AgInS_2$/P3HT/Pt hybrid solar cells, ZnS is a buffer layer, $AgInS_2$ is an inorganic sensitizer, and P3HT serves as both hole conductor and light absorber. Creating an effective energy gradient nanostructure can significantly improve the efficiency of charge injection and collection, and thus increase the photoelectric performance. The energy band structure of ITO/ZnO/ZnS/$AgInS_2$/P3HT is schematically illustrated in Figure 11. The lowest unoccupied molecular orbital (LUMO)

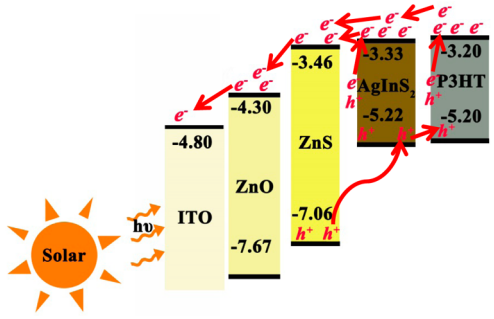

Figure 11. Schematic representation of energy gap structures of ZnO/ZnS/$AgInS_2$/P3HT.

level of P3HT (−3.20 eV) is higher than the conduction band edge of $AgInS_2$ (−3.33 eV). Hence, electrons injection from the LUMO of P3HT into the conduction band of $AgInS_2$ is energetically favorable, and thus the gradient energy band structure is very efficient on enhancing the separation and transportation of photoinduced electrons. In other words, the HOMO and the LUMO levels in P3HT are compatible with the conduction band of the $AgInS_2$, ZnS and ZnO to drive the charge transfer process.[26] Moreover, the valence band of

$AgInS_2$ (−5.22 eV) is lower than the HOMO level of both P3HT (−5.20 eV) and the valence band of ZnS is lower than that of $AgInS_2$, ensuring hole transport from $AgInS_2$ to P3HT and from ZnS to $AgInS_2$. $AgInS_2$ and ZnS act as a blocking layer by hindering the transfer of holes from P3HT to ZnS and hindering the transfer of holes from $AgInS_2$ to ZnO. Therefore, this gradient energy structure reduces the recombination of hole/electron and increases the charge carrier lifetime. In other words, both the ZnS buffer layer and the $AgInS_2$ sensitizer layer can promote separation of photoinduced electrons and holes, which remarkably decreases the dark current and benefit to the power conversion efficiency. Moreover, a buffer layer between core and shell can optimizes the band configuration by means of enhancing the excess carrier lifetime and improving the lattice matching in the heterojunction interface.[27] Interestingly, buffer layer between ZnO and $AgInS_2$ can not only promote the photoinduced electrons transfer from $AgInS_2$ to ZnO, but also accelerate the holes transfer from ZnO to $AgInS_2$. Electrochemical impedance spectroscopy (EIS) is an effective method to study the charge transport behavior in solid-state solar cells.[28] To investigate the carrier transport performance of ZnO/ZnS/Ag_2S NTs and ZnO/ZnS/$AgInS_2$ NTs, we determined electrochemical impedance spectroscopy (EIS) using electrochemical workstation. It is well-known that the electron lifetime is related to the recombination resistance, whereas the large semicircle radius of EIS means large electron/hole recombination resistance. In other words, the semicircle radius reflects the electron lifetime.[29,30] Figure 12 shows the

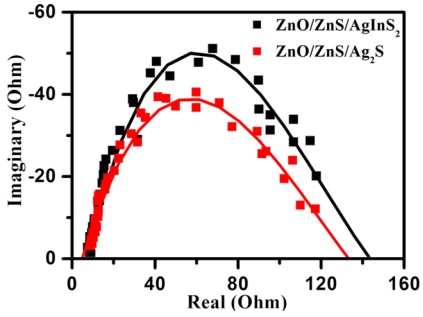

Figure 12. Electrochemical impedance spectroscopy of ZnO/ZnS/Ag_2S and ZnO/ZnS/$AgInS_2$.

electrochemical impedance spectroscopy (EIS) of ZnO/ZnS/Ag_2S and ZnO/ZnS/$AgInS_2$, it can be seen that the charge carrier lifetime in ZnO/ZnS/$AgInS_2$ is longer than that in ZnO/ZnS/Ag_2S, which results in the electron/hole recombination in ZnO/ZnS/$AgInS_2$ being less than that in ZnO/ZnS/Ag_2S. These EIS data demonstrate a gradient energy band structure was created by $AgInS_2$ modified ZnO nanoarrays, that is, the cascade energy band gap structure of ZnO/ZnS/$AgInS_2$ is more suitable for electrons collection and transportation compared with ZnO/ZnS/Ag_2S. The higher efficiency of $AgInS_2$-sensitized ZnO-based solar cell can be attributed to (i) ideal band gap value of $AgInS_2$, which is closely matched to the visible part of the solar spectrum; (ii) high light absorption coefficient of $AgInS_2$; (iii) appropriate conduction band and valence band location for constructing cascade energy gap structure. It should be noted to that the gradient energy band structure can enhance the separation and transportation of photoinduced electrons and holes dramatically. As a result, the appropriate matching of the energy band structures of ZnO/ZnS/$AgInS_2$/P3HT can improve the efficiency of transfer and separate of the photoinduced carriers and thus increase the power conversion efficiency.

In spite of rarely reported to date, $AgInS_2$ sensitized metal oxides would be widely developed as photoanodes in solar cells due to their excellent photoelectric properties. The next step of research can be focused on the optimization of photoelectric performance by means of (i) adjusting the amount of $AgInS_2$ for enhanced light absorption; (ii) preparing different morphology $AgInS_2$ with high specific surface area; (iii) exploiting other ideal sensitizer with ideal band gap and high light absorption coefficient, and coupling two kinds of sensitizer comodified metal oxide nanoarrays.

4. CONCLUSIONS

Vertically aligned double-walled ZnO/ZnS/$AgInS_2$ NT arrays were directly grown on ITO substrate using ZnO NRs as templates via a low-cost hydrothermal method. Chemical conversion method based on ion-exchange for fabricate well-aligned ZnO-based core/shell nanoarrays is easy to be manipulated and formed of uniform structure without destroying the original morphology. The large difference in product solubility constant plays a critical role in the chemical conversion process. The photoelectric properties of ZnO/ZnS/$AgInS_2$ photoelectrode are measured, the power conversion efficiency of ITO/ZnO/ZnS/$AgInS_2$/P3HT/Pt all-solid-state solar cell is 2.11% because of the improved absorption spectrum and appropriate gradient energy gap structure. These results suggest that the ternary $AgInS_2$ sensitizer is suitable for light-absorbing in solar cells, and the photoelectrode of ZnO/ZnS/$AgInS_2$ NT arrays described here presents excellent properties. Furthermore, this study will thus be important for designing and constructing uniform core/shell nanoarrays used in new type solar cells.

AUTHOR INFORMATION

Corresponding Authors

*E-mail: tjulzf@163.com.Tel: +86 22 23085236. Fax: +86 22 23085110.

*E-mail: yufengzhao@ysu.edu.cn. Tel: +86 3358061569. Fax: +86 3358061569.

Notes

The authors declare no competing financial interest.

ACKNOWLEDGMENTS

The authors gratefully acknowledge financial support from National Nature Science Foundation of China (51102174).

REFERENCES

(1) O'Regan, B.; Grätzel, M. A Low-cost, High-efficiency Solar Cell Based on Dye-sensitized Colloidal TiO_2 Films. *Nature* **1991**, *353*, 737−740.

(2) Brown, P. R.; Lunt, R. R.; Zhao, N.; Osedach, T. P.; Wanger, D. D.; Chang, L. Y.; Bawendi, M. G.; Bulović, V. Improved Current Extraction from ZnO/PbS Quantum Dot Heterojunction Photovoltaics using a MoO_3. *Interfacial Layer Nano Lett.* **2011**, *11*, 2955−2961.

(3) Liu, Z. F.; Han, J. H.; Han, L.; Guo, K. Y.; Li, Y. J.; Cui, T.; Wang, B.; Liang, X. P. Fabrication of ZnO/CuS Core/Shell Nanoarrays for Inorganic-Organic Heterojunction Solar. *Cells Mater. Chem. Phys.* **2013**, *141*, 804−809.

(4) Chen, T. T.; Chang, I. C.; Yang, M. H.; Chiu, H. T.; Lee, C. Y. The Exceptional Photo-catalytic Activity of ZnO/RGO Composite via Metal and Oxygen Vacancies. *Appl. Catal., B* **2013**, *142−143*, 442−449.

(5) Han, J. H.; Liu, Z. F.; Zheng, X. R.; Guo, K. Y.; Zhang, X. Q.; Hong, T. T.; Wang, B.; Liu, J. Q. Trilaminar ZnO/ZnS/Sb_2S_3 Nanotube Arrays for Efficient Inorganic-organic Hybrid Solar. *Cells RSC Adv.* **2014**, *4*, 23807−23814.
(6) Zhang, Y. C.; Yang, M.; Zhang, G. S.; Dionysiou, D. D. HNO_3-involved One-step Low Temperature Solvothermal Synthesis of N-doped TiO_2 Nanocrystals for Efficient Photocatalytic Reduction of Cr(VI) in Water. *Appl. Catal., B* **2013**, *142*−*143*, 249−258.
(7) Zhang, Y. C.; Li, J.; Xu, H. Y. One-step in Situ Solvothermal Synthesis of SnS_2/TiO_2 Nanocomposites with High Performance in Visible Light-driven Photocatalytic Reduction of Aqueous Cr(VI). *Appl. Catal., B* **2012**, *123*−*124*, 18−26.
(8) Chen, X. P.; Chen, W.; Gao, H. Y.; Yang, Y.; Shangguan, W. F. In Situ Photodeposition of NiO_x on CdS for Hydrogen Production under Visible Light: Enhanced Activity by Controlling Solution Environment. *Appl. Catal., B* **2014**, *152*−*153*, 68−72.
(9) Antoniadou, M.; Daskalaki, V. M.; Balis, N.; Kondarides, D. I.; Kordulis, C.; Lianos, P. Photocatalysis and Photoelectrocatalysis using (CdS-ZnS)/TiO_2 Combined Photocatalysts. *Appl. Catal., B* **2011**, *107*, 188−196.
(10) Reiss, P.; Protière, M.; Li, L. *Core/Shell Semiconductor Nanocrystals Small* **2009**, *2*, 154−168.
(11) Huo, Y. N.; Yang, X. L.; Zhu, J.; Li, H. X. Highly Active and Stable CdS-TiO_2 Visible Photocatalyst Prepared by in Situ Sulfurization under Supercritical Conditions. *Appl. Catal., B* **2011**, *106*, 69−75.
(12) Li, Y.; Lu, P. F.; Jiang, M. L.; Dhakal, R.; Thapaliya, P.; Peng, Z. H.; Jha, B.; Yan, X. Z. Femtosecond Time-Resolved Fluorescence Study of TiO_2-Coated ZnO Nanorods/P3HT Photovoltaic Films. *J. Phys. Chem. C* **2012**, *116*, 25248−25256.
(13) Chen, D. W.; Wang, T. C.; Liao, W. P.; Wu, J. J. Synergistic Effect of Dual Interfacial Modifications with Room-Temperature-Grown Epitaxial ZnO and Absorbed Indoline Dye for ZnO Nanorod Array/P3HT Hybrid Solar Cell ACS. *ACS Appl. Mater. Interfaces* **2013**, *5*, 8359−8365.
(14) Torimoto, T.; Tada, M.; Dai, M.; Kameyama, T.; Suzuki, S.; Kuwabata, S. Tunable Photoelectrochemical Properties of Chalcopyrite $AgInS_2$ Nanoparticles Size-Controlled with a Photoetching Technique. *J. Phys. Chem. C* **2012**, *116*, 21895−21902.
(15) Li, X. M.; Niu, J. Z.; Shen, H. B.; Xu, W. W.; Wang, H. Z.; Li, L. S. Shape Controlled Synthesis of Tadpole-like and Heliotrope Seed-like $AgInS_2$. *Nanocrystals CrystEngComm* **2010**, *12*, 4410−4415.
(16) Liu, Z. P.; Tang, K. B.; Wang, D. K.; Wang, L. L.; Hao, Q. Y. Facile Synthesis of $AgInS_2$ Hierarchical Flowerlike Nanoarachitectures Composed of Ultrathin Nanowires. *Nanoscale* **2013**, *5*, 1570−1575.
(17) Mamidala, V.; Nalla, V.; Maiti, P. S.; Valiyaveettil, S.; Ji, W. Charge Transfer Assisted Nonlinear Optical and Photoconductive Properties of CdS-$AgInS_2$ Nanocrystals Grown in Semiconducting Polymers. *J. Appl. Phys.* **2013**, *113*, 123107.
(18) Li, Y. B.; Liu, Z. F.; Wang, Y.; Liu, Z. C.; Han, J. H.; Ya, J. ZnO/$CuInS_2$ Core/Shell Heterojunction Nanoarry for Photoelectrochemical Water Splitting Int. *J. Hydrogen Energy* **2012**, *37*, 15029−15037.
(19) Liu, Z. F.; E, L.; Ya, J.; Xin, Y. Growth of ZnO Nanorods by Aqueous Solution Method with Electrodeposited ZnO Seed Layers. *Appl. Surf. Sci.* **2009**, *255*, 6415−6420.
(20) Xu, J.; Luan, C. Y.; Tang, Y. B.; Chen, X.; Zapien, J. A.; Zhang, W. J.; Kwong, H. L.; Meng, X. M.; Lee, S. T.; Lee, C. S. Low-Temperature Synthesis of $CuInSe_2$ Nanotube Array on Conducting Glass Substrates for Solar Cell Application. *ACS Nano* **2010**, *4*, 6064−6070.
(21) Shuai, X. M.; Shen, W. Z. A Facile Chemical Conversion Synthesis of ZnO/ZnS Core/Shell Nanorods and Diverse Metal Sulfide Nanotubes. *J. Phys. Chem. C* **2011**, *115*, 6415−6422.
(22) Liu, Z. F.; Liu, C. C.; Ya, J.; E, L. Controlled Synthesis of ZnO and TiO_2 Nanotubes by Chemical Method and Their Application in Dye-sensitized Solar Cells. *Renew. Energy* **2011**, *36*, 1177−1181.
(23) She, G. W.; Zhang, X. H.; Shi, W. S.; Fan, X.; Chang, J. C.; Lee, C. S.; Lee, S. T.; Liu, C. H. Controlled Synthesis of Oriented Single-Crystal ZnO Nanotube Arrays on Transparent Conductive Substrates. *Appl. Phys. Lett.* **2008**, *92*, 053111.
(24) Wu, J. J.; Chen, Y. R.; Liao, W. P.; Wu, C. T.; Chen, C. Y. Construction of Nanocrystalline Film on Nanowire Array via Swelling Electrospun Polyvinylpyrrolidone- Hosted Nanofibers for Use in Dye-sensitized Solar Cells. *ACS Nano* **2010**, *4*, 5679−5684.
(25) Barbé, C. J.; Arendse, F.; Comte, P.; Jirousek, M.; Lenzmann, F.; Shklover, V.; Grätzel, M. Nanocrystalline Titanium Oxide Electrodes for Photovoltaic Applications. *J. Am. Cream. Soc.* **1997**, *80*, 3157−3171.
(26) Chang, J. A.; Rhee, J. H.; Im, S. H.; Lee, Y. H.; Kim, H. J.; Seok, S. I.; Nazeeruddin, M. K.; Grätzel, M. High-Performance Nanostructured Inorganic-Organic Heterojunction Solar. *Cells Nano Lett.* **2010**, *10*, 2609−2612.
(27) Lee, D.; Yong, K. Superstrate $CuInS_2$ Photovoltaics with Enhanced Performance using a CdS/ZnO Nanorod Array ACS. *Appl. Mater. Inter.* **2012**, *4*, 6758−6765.
(28) Santiago, F. F.; Bisquert, J.; Cevey, L.; Chen, P.; Wang, M.; Zakeeruddin, S. M.; Grätzel, M. Electron Transport and Recombination in Solid-State Dye Solar Cell with Spiro-OMeTAD as Hole Conductor. *J. Am. Chem. Soc.* **2009**, *131*, 558−562.
(29) Hsu, S. C.; Liao, W. P.; Lin, W. H.; Wu, J. J. Modulation of Photocarrier Dynamics in Indoline Dye-modified TiO_2 Nanorod Array/P3HT Hybrid Solar Cell with 4-tert-butylpridine. *J. Phys. Chem. C* **2012**, *116*, 25721−25726.
(30) Wu, W. Q.; Xu, Y. F.; Rao, H. S.; Su, C. Y.; Kuang, D. B. Multistack Integration of Three-Dimensional Hyperbranched Anatase Titania Architectures for High-efficiency Dye-sensitized Solar Cells. *J. Am. Chem. Soc.* **2014**, *136*, 6437−6445.